BULLETIN OF THE POLISH ACADEMY OF SCIENCES
TECHNICAL SCIENCES, Vol. 70(2), 2022, Article number: e140372
DOI: 10.24425/bpasts.2022.140372

Reliability assessment of the port power system based on integrated energy hybrid system

Liang FANG[1], Xiao-Yan XU[2], Jun XIA[3], and Tomasz TARASIUK[4]*

[1] Shanghai Maritime University, Shanghai, 201305, China
[2] Marine Design & Research Institute of China, Shanghai, 201305, China
[3] Gdynia Maritime University, 81-225 Gdynia, Poland

Abstract. The conventional port distribution power system is being disrupted by increasing distributed generation (DG) levels based on integrated energy. Different new energy resources combine with conventional generation and energy storage to improve the reliability of the systems. Reliability assessment is one of the key indicators to measure the impact of the distributed generation units based on integrated energy. In this work, an analytical method to investigate the impacts of using solar, wind, energy storage system (ESS), combined cooling, heating and power (CCHP) system and commercial power on the reliability of the port distribution power system is improved, where the stochastic characteristics models of the major components of the new energy DG resources are based on Markov chain for assessment. The improved method is implemented on the IEEE 34 Node Test Feeder distribution power system to establish that new energy resources can be utilized to improve the reliability of the power system. The results obtained from the case studies have demonstrated efficient and robust performance. Moreover, the impacts of integrating DG units into the conventional port power system at proper locations and with appropriate capacities are analyzed in detail.

Key words: Markov model; distributed generation; reliability assessment; integrated energy; distribution power system.

1. INTRODUCTION

Low-carbon emission and efficient and reliable operation of various energy resources and storage systems are the main topics in research on power systems. This leads to integrated energy systems (IES), which comprises electricity, natural gas, heating/cooling, and other energy resources. One solution may be the introduction of technologies behind microgrid and IES concepts into port energy infrastructure [1]. In some respects, this can be extended to the IES concept. However, the level of the system complexity increases with the inclusion of local, renewable sources, stand-by and emergency sources, and energy storage devices [2]. One must also remember that the demand varies during various port facilities operations, including shore-to-ship supply systems. Therefore, requirements for the safety and reliability of the port systems increase.

IES directly connects the various energy consumers and different forms of energy with flexible topological structures. This concept makes the interdependence of subsystems possible and leads to a reliability problem since the intermittent and volatile character of wind/solar energy negatively impacts the reliability of port distributed power grids. Reliability is the probability that a power system will perform its functions under normal operating conditions without failure within a stipulated period [2]. The purpose of the reliability analysis is to assess a failure impact on components and systems, thereby improving the design or preventing unacceptable consequences for port distributed power systems [3].

In the past, efforts were mainly concentrated on the reliability assessment for simple subsystems, such as electricity, natural gas, wind/solar and other systems [4,5]. Therefore, research for an accurate reliability assessment is required for a port distributed power system based on integrated energy.

Several methodologies have been proposed for the aim. The impact of renewable distributed generation and energy storage units on a conventional distribution system's reliability has been studied in [6]. Li *et al.* [7] have proposed a security-constrained bi-level economic dispatch model for an integrated natural gas and electrical system considering wind power and a power-to-gas process. Despite these efforts, the reliability evaluation of IES is still at an early stage. Gonzalez *et al.* [8] have performed a novel approach to evaluate a power system's renewable energy accommodation capacity with wind power and photovoltaic integration. At the same time, the new concept of weather influence factor is presented to reflect the uncertainty of wind and photovoltaic output. Das *et al.* [9] have carried out a feasibility and techno-economic analysis of stand-alone and grid integration with different system configurations of photovoltaic, wind, diesel and battery energy sources based on the hybrid energy system for five different climatic regions by using a hybrid optimization model for electric renewables. The case results proved that a photovoltaic/wind/diesel/battery hybrid energy system is more efficient and reliable for the region than the stand-alone system.

*e-mail: t.tarasiuk@we.umg.edu.pl

Manuscript submitted 2021-07-19, revised 2021-09-25, initially accepted for publication 2021-10-16, published in April 2022.

A multi-objective function is proposed in [10] to determine the optimal locations to place DGs in the distribution system to enhance reliability and voltage profile. Moreover, the impact of variable distributed energy resources capacity penetration levels on system reliability and voltage profile improvement is also analyzed. A new method for optimal allocation of DG units in the transmission systems is proposed in [11] based on operational indices to improve reliability.

In the literature, several methods are available to calculate network reliability. The Monte Carlo simulation technique has been used to estimate reliability indices [12]. The Monte Carlo simulation results illustrate that the stochastic behavior of the new energy technologies plays an important role in determining the reliability indices. This method takes up large computational times when applied to the large electrical power networks that contain multi-objective functions.

Large systems are characterized by an extensive number of Markov states, resulting in a necessity to replace analytical methods with simulation programs. A method for assessing the current reliability of a power system with an equivalent model based on a Markov chain was proposed by Wang *et al.* [13]. Al-Muhaini and Heydt [14] presented the reduction and truncation techniques to overcome problems associated with the use of a large number of components and states in Markov matrices. This method yields more information on the load points and system reliability indices when compared to the Monte Carlo simulation. Although many approaches have been proposed to improve the reliability assessment of a conventional distribution system, the stochastic character of the wind/solar units and their impact on the reliability assessment have not been fully addressed.

The reliability model presented in this paper is intended for port power system reliability evaluation, and it is based on Markov chains. This paper aims to consider the new energy sources in conjunction with their stochastic characteristics to enhance the reliability assessment of the port power system. Reliability models are developed for wind/solar energy, energy storage and natural gas-to-power systems. Analytical algorithms are designed to calculate reliability indices. The main contributions are as follows:

1. Development of a model with energy distributed generation units that will assess the reliability of port power systems based on the integrated energy concept.
2. Application of a Markov model of the distribution power system, taking into account the stochastic characteristics of DG units.
3. Assessment of the benefits of using integrated energy systems in ports, the effect of the voltage profile on the reliability analysis is also investigated.

2. PORT DISTRIBUTED GENERATION SYSTEM

There is no internationally accepted definition of DG. DG has been described as being small scale [15], is an electric distribution system that can operate within or independent of the entire power network. Different new energy resources combine with conventional generation and energy storage to improve the systems' reliability reduce cost. This opens new possibilities for the systems control and operation to improve their efficiency and leads to new problems with their design and reliability assessment.

In this paper, the proposed port distribution power system consists of wind/solar and energy storage systems combined with cooling, heating, and conventional systems, including commercial systems. It is designed to meet the port load requirements and the system constraints. Owing to the fact that wind and solar power output changes with time, the power generated from the systems must be stored in the energy storage system, which will reduce the power outage time and increase the efficiency of the port power system [16]. This section briefly presents the modelling of the new DG system, including solar, wind, energy storage systems and CCHP system. It provides basic information about the characteristics of these systems, particularly the impact of weather factors.

2.1. Solar system

Recent technical and economic advances have made solar energy a practical alternative for electric power generation. In China, most coastal ports are located in regions with abundant solar energy resources suitable for the construction of solar energy generation projects, where the average yearly global solar radiation is about 1349.44 kWh/m^2 [17]. As a new energy source, solar systems have great potential for satisfying increasing energy needs in ports. Unlike other new energy sources, the solar system enables us to take advantage of existing building surfaces to produce energy onsite where it is required [18]. Moreover, the power output of a PV system depends on the sun's location in the sky, solar radiance and operating temperature [19]. The output of the solar system can be expressed as [20]:

$$\begin{cases} T_c = T_a + I_\beta \cdot \left\{ \dfrac{N_{ot} - 20}{0.8} \right\}, \\ I = I_\beta \cdot \{ I_{sc} + K_c \cdot (T_c - 25) \}, \\ V = V_{oc} - K_v \cdot T_c, \\ FF = (V_{mp} \cdot I_{mp}) / (V_{oc} \cdot I_{sc}), \\ P_{pv}(I_\beta) = N \cdot FF \cdot V \cdot I, \end{cases} \tag{1}$$

where T_c is the cell temperature, T_a is the ambient temperature, N_{ot} is the nominal cell operating temperature, V_{oc} is the open-circuit voltage, I_{sc} is the short circuit current, V_{mp} and I_{mp} are the voltage at maximum power and the current at maximum power, K_i and K_v are the current temperature coefficient and the voltage temperature coefficient respectively, while FF is the fill factor.

2.2. Wind system

Nowadays, wind energy plays an increasing role in providing electricity worldwide due to its advantage as a clean energy source. Next, offshore wind energy systems have a clear advantage compared to onshore generation, like higher wind speed, more flexible locations and lesser concerns around turbine noise [21]]. Port areas have the natural geographical ad-

vantages for a wind generation system. The output power of the wind system depends on the wind speed, swept area of the rotor, air density, aero-turbine and efficiency of gearbox and generator, etc. The mathematical expression for estimation of the power output of the wind system is presented in (2) [22]:

$$P_w(v(t)) = \begin{cases} 0 & v(t) < v_{ci} \text{ or } v(t) > v_{co} \\ P_{\text{rated}} \dfrac{v(t) - v_{ci}}{v_r - v_{ci}} & v_{ci} \le v(t) \le v_r\,, \\ P_{\text{rated}} & v_r \le v(t) \le v_{co}\,, \end{cases} \tag{2}$$

where P_{rated} is the rated power output of the wind turbine, v_{ci} is the cut-in wind speed, v_r is the rated wind speed, v_{co} is the cut-out wind speed, and P_w is the power output of the wind speed.

2.3. Energy storage system

Since new energy resources are naturally intermittent, an energy storage system is required to optimize their energy utilization [23]. The main role of ESS in a DG is to maintain stability, facilitate the integration of the new energy and improve power quality. Fast response ESS can damp electromechanical oscillations in power systems because they can provide storage capacity in addition to the kinetic energy of generators with the ability for sharing sudden changes in power [24]. The batteries act as an energy storage subsystem modelled as a single equivalent battery. The energy balance defines the batteries state of charge E_{bin} in kWh [24]:

$$E_{\text{bat}}(t) = E_{\text{bat}}(t-1) + E_{\text{bin}}(t) \cdot (\eta_{BC} - \eta_{AD}) - \frac{E_{\text{bout}}(t)}{\eta_{BD} \cdot \eta_{DA}} \quad \forall t, \tag{3}$$

where $E_{\text{bout}}(t)$ is the energy used from the batteries, $E_{\text{bin}}(t)$ is the energy available to charge the batteries in the time step t, η_{BC} and η_{BD} are the batteries' charge and discharge efficiency, η_{AD} is the power equipment efficiency in AC-DC and η_{DA} is power equipment efficiency in DC-AC.

2.4. CCHP system

A typical CCHP system with hybrid chillers consists of a power generation unit (PGU), a heat recovery system, an absorption chiller, an electric chiller, a heating coil and a boiler [25]. CCHP system can be interconnected to DG system due to a stable supply of natural gas. Thus, the operational stability and economic efficiency of DG system can be greatly improved. Coordination of the CCHP system operation and the port distribution power system is essential for improving economic efficiency, reducing pollutant emissions and alleviating the uncertainties of renewable sources and load demands. The electrical energy balance is as follows [26]:

$$\begin{aligned} E_{\text{grid}} &= E_d + E_{ec} + E_s - E_{pgu}E_{pgu} < E_d + E_{ec} + E_s \\ E_{\text{excess}} &= E_{pgu} - E_d - E_{ec} - E_s E_{pgu} \ge E_d + E_{ec} + E_s\,, \end{aligned} \tag{4}$$

where E_{grid} and E_{excess} are the amounts of electrical energy sent from the grid and the excess electricity produced by the PGU that can be sold back to the grid. E_{pgu} is the electrical energy generated by the PGU, and E_d is the electrical energy demand, while E_{ec} and E_s are the electrical energy amounts supplied to the electric chiller and consumed by the CCHP system.

2.5. Integrated energy hybrid system

The balance between the amount of energy that is used, including demand, plus the remaining charge values of the batteries and the available energy, including wind/solar/batteries discharge/CCHP/commercial power energy, is as follows:

$$E_{\text{dem}}(t) + E_{\text{bat}}(t) = E_{pv}(t) + E_w(t) + E_{pgu}(t) + E_{\text{bout}}(t) + E_{cp}(t), \quad \forall t, \tag{5}$$

where $E_{\text{dem}}(t)$ is the loads power demands, $E_{\text{ban}}(t)$ is the energy to charge the batteries, $E_{pv}(t)$ and $E_w(t)$ are the used energy from the wind and solar systems. $E_{pgu}(t)$ is the energy produced by the CCHP system, $E_{\text{bout}}(t)$ is the energy used from the batteries and $E_{cp}(t)$ is the power supplied by the power utilities.

3. RELIABILITY ASSESSMENT OF PORT POWER SYSTEM

The reported power outages in the distribution systems are about 80% of the total outages in the port power system. Consequently, the port power system requires a reliable power supply for power outages, and reliability assessment is vital for the system operation.

The failure of distribution components causes service interruptions, thereby decreasing system reliability. In this study, the reliability of the port distributed power system is evaluated using the Markov method analysis. A flowchart of the reliability assessment for the port power system is depicted in Fig. 1. The impacts of the DG system on the port power system's reliability are compared by using different combinations of wind energy, solar energy, ESS, CCHP and commercial power.

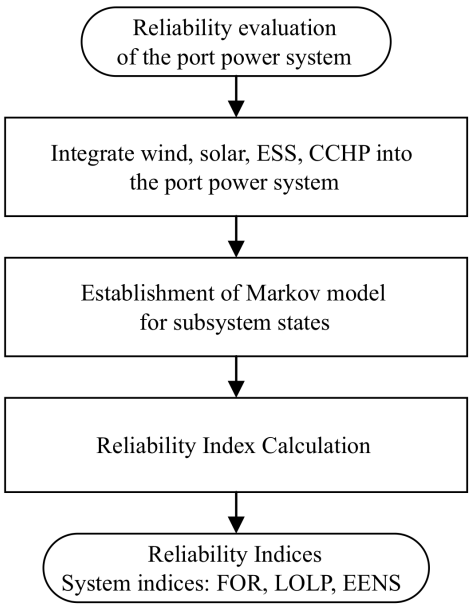

Fig. 1. Reliability evaluation flow char

This section provides a concise and precise description of the experimental results, their interpretation and conclusions.

3.1. Time-varying failure rate model

Traditional reliability assessment ignores the impact of operation life, maintenance plan, and other factors on the equipment failure rate and considers the equipment failure rate constant. It was shown that this Weibull distribution function could describe the failure rate curve of equipment [27]. The used Weibull distribution function can be expressed as:

$$\lambda(t) = kt^{\beta-1}, \tag{6}$$

where k is the scale parameter (initial failure rate, the failure rate distribution curve is continuous in time), β is the shape parameter. The two-parameter Weibull model ($\lambda(t) = mt^{m-1}/\eta^m$) is influenced by shape parameters m and scale parameters η. Considering that the failure rate curve of the equipment is in the shape of a bathtub, function (6) can more vividly express the failure rate curve of the equipment.

The average failure rate replaces the time-varying failure rate of the equipment lacking failure statistics. The modified one-parameter Weibull distribution function can be presented in (7) as:

$$\lambda(T) = \begin{cases} \lambda_{\text{avg}} e^{\beta_0 T} & 0 < T \le T_0, \\ \lambda_{\text{avg}} e^{\beta_1 T} & T_0 < T \le T_1, \\ \lambda_{\text{avg}} e^{\beta_2 T} & T_1 < T \le T_2, \end{cases} \tag{7}$$

where λ_{avg} is constant, that means the average failure rate, β_0 is the shape parameter in the initial period T_0, β_1 is the shape parameter in a stable period T_1, and β_2 is the shape parameter in wear-out failure period T_2. In the initial failure phase $0 < T < T_0$, $\beta = \beta_0 < 0$, the time-varying failure rate decreases with an increase of the service life T, where the failure rate only changes with the service life of the equipment and its value is constant in the reliability evaluation of a certain year. The time-varying failure rate is constant in a stable period $T_0 < T < T_1$, $b = b_1 = 0$. In wear-out failure period $T_1 < T < T_2$, $\beta = \beta_0 > 0$, the time-varying failure rate increases with the increase of the service life T.

The weather is another important factor that makes components wear out. The time-varying failure rate for the entire model is obtained by using the equations:

$$\lambda(t) = \left[\lambda(T)\right]^{\theta(t)}, \tag{8}$$

where $\theta(t)$ is the weather factor.

3.2. Markov reliability model

Markov chains are used to model a sequence of discrete or continuous random variables that correspond to a set of system states [28]. A state transition matrix can mathematically represent the states and transition probabilities. For a system with n discrete states, $S_1, S_2, \ldots, S_n$ and ρ_{ij} determine the transition from one state to another.

Most components can be denoted in a power system in two states: up and down. It is assumed that states i and j, respectively, are both up and down states. Consequently, the transition ρ_{ij} from the up state to the down state is equivalent to the failure rate ($\lambda_{ij}(t)$), while the transition ρ_{ij} from the down state to the up state corresponds to the repair rate (μ_{ij}). System states are classified as either an up or down state based on the individual components that constitute the system.

3.2.1. Markov model for the solar system

The solar system has three important components. These are an array of PV models, a DC/DC booster converter and a DC/AC inverter. The effect of other components of this subsystem can be neglected for reliability studies. The system can be represented in two states: up state and down state. Up state indicates that all components of the system are running properly. Down state indicates that some components of the system are faulty or in a non-operating state. In contrast, non-operating state indicates that some system components are in a derating state. Figure 2 shows the Markov model for the PV modules, DC/DC booster converter and DC/AC inverter with eight states.

Between the two states of PV modules, the DC/DC booster converter and DC/AC inverter are represented by 1 and 0, respectively. The running state of the whole system depends on the state characteristics of the system's main components. In Fig. 2, states 1–8 are the solar system's operating states un-

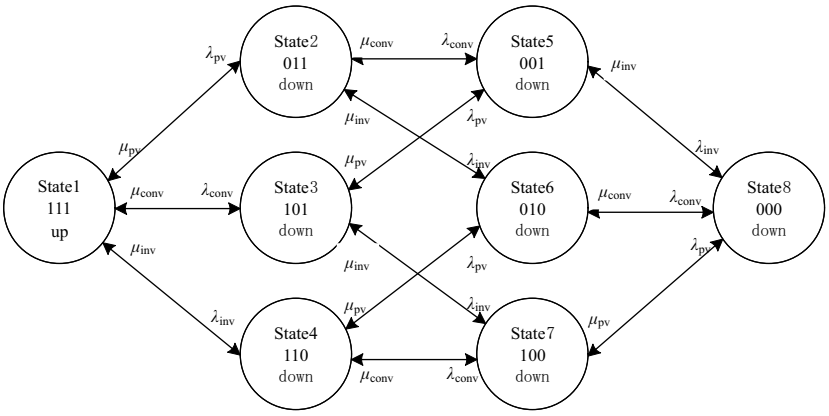

Fig. 2. Stochastic model for the solar system

der different working states of each component. When the PV modules, DC/DC booster converter and DC/AC inverter are all in the 'up state' that is state 1 in Fig. 2, the whole solar system can operate normally. When any solar system component is in the "down state" that is states 2-State 8 in Fig. 2, the whole solar system is in stagnation or failure state. Therefore, the system's random probability matrix determines that the system can only run normally when it is in state 1, and the system is in a state of stagnation or failure when it is in states 2–8. Equation (9) gives the stochastic probability matrix for the architecture shown below.

$$P = \begin{bmatrix} \lambda_a(t) & \lambda_{pv}(t) & \lambda_{bc}(t) & \lambda_i(t) & 0 & 0 & 0 & 0 \\ \mu_{pv} & \lambda_b(t) & 0 & 0 & \lambda_{bc}(t) & 0 & \lambda_i(t) & 0 \\ \mu_{bc} & 0 & \lambda_c(t) & 0 & \lambda_{pv}(t) & \lambda_i(t) & 0 & 0 \\ \mu_i & 0 & 0 & \lambda_d(t) & 0 & \lambda_{bc}(t) & \lambda_{pv}(t) & 0 \\ 0 & \mu_{bc} & \mu_{pv} & 0 & \lambda_e(t) & 0 & 0 & \lambda_i(t) \\ 0 & 0 & \mu_i & \mu_{bc} & 0 & \lambda_f(t) & 0 & \lambda_{bc}(t) \\ 0 & \mu_i & 0 & \mu_{pv} & 0 & 0 & \lambda_g(t) & \lambda_{pv}(t) \\ 0 & 0 & 0 & 0 & \mu_i & \mu_{pv} & \mu_{bc} & \lambda_h(t) \end{bmatrix}$$

$$\begin{cases} \lambda_a(t) = 1 - \lambda_{pv}(t) - \lambda_{bc}(t) - \lambda_i(t) \\ \lambda_b(t) = 1 - \mu_{pv} - \lambda_{bc}(t) - \lambda_i(t) \\ \lambda_c(t) = 1 - \lambda_{pv}(t) - \mu_{bc} - \lambda_i(t) \\ \lambda_d(t) = 1 - \lambda_{pv}(t) - \lambda_{bc}(t) - \mu_i \\ \lambda_e(t) = 1 - \mu_{pv} - \mu_{bc} - \lambda_i(t) \\ \lambda_f(t) = 1 - \mu_{bc} - \mu_i - \lambda_{bc}(t) \\ \lambda_g(t) = 1 - \mu_{pv} - \mu_i - \lambda_{pv}(t) \\ \lambda_h(t) = 1 - \mu_{pv} - \mu_{bc} - \mu_i \end{cases} \tag{9}$$

where $\lambda_{pv}(t)$, μ_{pv}, $\lambda_{pv}(t)$, μ_{bc}, $\lambda_{pv}(t)$ and μ_i are the time-varying failure rates and repair rates of the PV modules, DC/DC booster converter and DC/AC inverter.

The state probability matrix shows the probability of the system residing in one of the states shown in Fig. 2. The solar system will operate if all components are operable, otherwise states 2–8 being a failure can be represented by absorbing states which results in equation (10) as a truncated matrix.

$$[Q] = [1 - \lambda_{pv}(t) - \lambda_{bc}(t) - \lambda_i(t)], \tag{10}$$

It can be assumed that the failure rate only varies with the operating life of the equipment. When the reliability is evaluated for a certain year, its value is constant. Therefore, the meantime to failure (*MTTF*) for the solar system can be obtained by using the following steps:

$$\begin{aligned} MTTF &= [I - Q]^{-1} = [[I] - [1 - \lambda_{pv}(t) - \lambda_{bc}(t) - \lambda_i(t)]]^{-1} \\ &= [\lambda_{pv}(t) + \lambda_{bc}(t) + \lambda_i(t)]^{-1} \\ &= \frac{1}{\lambda_{pv}(t) + \lambda_{bc}(t) + \lambda_i(t)}, \end{aligned} \tag{11}$$

where I – the identity matrix.

Thus, the composite time-varying failure rate for the solar system can be expressed as:

$$\lambda_1(t) = \frac{1}{MTTF} = \lambda_{pv}(t) + \lambda_{bc}(t) + \lambda_i(t), \tag{12}$$

where $\lambda_1(t)$ is the composite time-varying failure rate for the solar system.

The Markov state transition diagram is presented in Fig. 2 where the time-varying failure rate and repair rate are represented by $\lambda(t)$ and μ, respectively. The probability of the solar system in the up state can be presented as follows:

$$P_{up} = \frac{\mu}{\lambda(t) + \mu}. \tag{13}$$

The probability of the PV modules, DC/DC booster converter and DC/AC inverter in their up states can be denoted as:

$$P_{up} = \frac{\mu_{pv}}{\mu_{pv} + \lambda_{pv}(t)} \frac{\mu_{bc}}{\mu_{bc} + \lambda_{bc}(t)} \frac{\mu_i}{\mu_i + \lambda_i(t)} = \frac{\mu_1}{\mu_1 + \lambda_1(t)}, \tag{14}$$

where μ_1 is the composite repair rate for the solar system.

The composite repair rate for the solar system is determined using (15):

$$\mu_1 = \frac{\lambda_1(t)}{\left[\left(1 + \frac{\lambda_{pv}(t)}{\mu_{pv}}\right)\left(1 + \frac{\lambda_{bc}(t)}{\mu_{bc}}\right)\left(1 + \frac{\lambda_i(t)}{\mu_i}\right) - 1\right]}, \tag{15}$$

3.2.2. Markov model for the wind system

The wind system consists of three major components: the wind turbine generator, an AC/DC rectifier, and a DC/AC inverter. The stochastic characteristics of the wind system components are used in this research to investigate their impacts on the reliability of the port power system. The Markov model for the wind system is presented in Fig. 3. The system can be represented by a two states model, such as the up and down states of each system component. The up and down states are represented by 1 and 0, respectively, in Fig. 3. When the wind turbine generator, an AC/DC rectifier and a DC/AC inverter of the wind system are all in the "up state", it is indicated by "111" (state1) to show that the whole wind system is operational. If any component of the wind system is in the "down state", it refers to States 2–8, and the wind system is non-operational. Therefore, the wind system is operational only if the three components are operable. A similar approach can be used to obtain the wind system's generating model.

According to formula (10)–(14), the composite time-varying failure rate and composite failure rate for the wind system can be evaluated as follows:

$$\lambda_2(t) = \lambda_w(t) + \lambda_r(t) + \lambda_i(t), \tag{16}$$

$$\mu_2 = \frac{\lambda_2(t)}{\left[\left(1 + \frac{\lambda_w(t)}{\mu_w}\right)\left(1 + \frac{\lambda_r(t)}{\mu_r}\right)\left(1 + \frac{\lambda_i(t)}{\mu_i}\right) - 1\right]}, \tag{17}$$

where $\lambda_2(t)$ and μ_2 are the composite time-varying failure rate and composite repair rate for the wind system, $\lambda_w(t)$, μ_w, $\lambda_r(t)$,

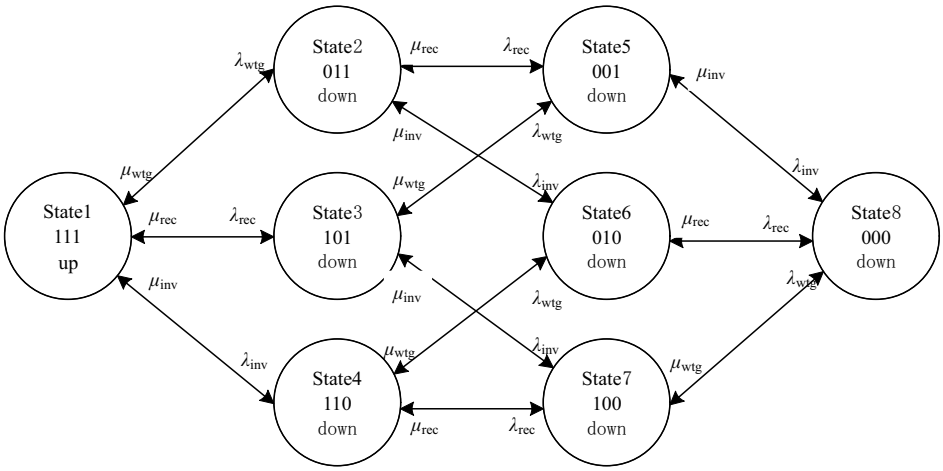

Fig. 3. Stochastic model for the wind system

μ_r, $\lambda_i(t)$ and μ_i are the time-varying failure rate and repair rate of the wind turbine generator, AC/DC rectifier and DC/AC inverter.

3.2.3. Markov model for the ESS system

The ESS system comprises of battery, charge controller and inverter system. Other components of this subsystem can be neglected for reliability research. Figure 4 shows the Markov model for the ESS system. The battery, charge controller and inverter system of the ESS system include the up and down states. Up and down states are represented by 1 and 0, respectively, in Fig. 4. When each system component is all in the 'up state' that means '111' (state1), the entire ESS system is operational. If any component of the ESS system is in the 'down state', this indicates System states 2–8 and the system is non-operational. Therefore, the ESS system is operational only if the three components are operable.

The composite time-varying failure rate and composite failure rate for the ESS system can be derived as follows:

$$\lambda_3(t) = \lambda_{\text{bat}}(t) + \lambda_{cc}(t) + \lambda_i(t), \tag{18}$$

$$\mu_3 = \frac{\lambda_3(t)}{\left[\left(1+\frac{\lambda_{\text{bat}}(t)}{\mu_{\text{bat}}}\right)\left(1+\frac{\lambda_{cc}(t)}{\mu_{cc}}\right)\left(1+\frac{\lambda_i(t)}{\mu_i}\right)-1\right]}, \tag{19}$$

where $\lambda_3(t)$ is the composite time-varying failure rate for the ESS system, μ_3 is the composite repair rate for the ESS system, $\lambda_{\text{bat}}(t)$, μ_{bat}, $\lambda_{dc}(t)$, μ_{dc}, $\lambda_i(t)$ and μ_i are the time-varying failure rate and repair rates of the battery, charge controller and inverter respectively.

3.2.4. Markov model for the CCHP system

The CCHP system has two major components: the gas turbine and generator. The failure of any components will cause the failure of the CCHP system. The Markov model for the CCHP system is shown in Fig. 5. The gas turbine and generator's up state and down state are represented by 0 and 1, respectively. If any component of the CCHP system is in the "down state", this indicates System states 2–4 and the system will not operate. The system will operate only if it is in state 1. The transition

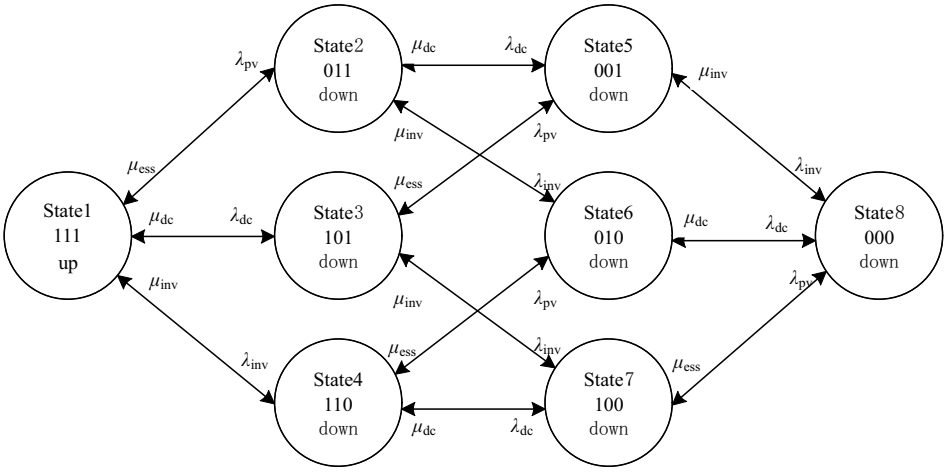

Fig. 4. Stochastic model for the ESS system

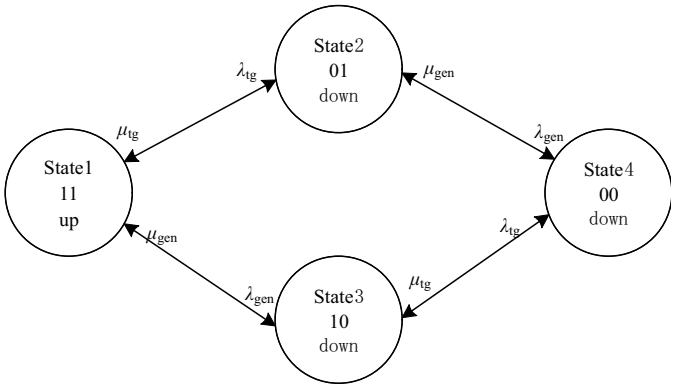

Fig. 5. Stochastic model for the CCHP system

probability matrix for the proposed system is shown below.

$$P_c = \begin{bmatrix} p_{11} & \lambda_{gen}(t) & \lambda_{gt}(t) & 0 \\ \mu_{gen} & p_{22} & 0 & \lambda_{gt}(t) \\ \mu_{gt} & 0 & p_{33} & \lambda_{gen}(t) \\ 0 & \mu_{gt} & \mu_{gen} & p_{44} \end{bmatrix}, \tag{20}$$

where

$$\begin{aligned} p_{11} &= 1 - \lambda_{gt}(t) - \lambda_{gen}(t). \\ p_{22} &= 1 - \lambda_{gt}(t) - \mu_{gen}(t). \\ p_{33} &= 1 - \mu_{gt}(t) - \lambda_{gen}(t). \\ p_{44} &= 1 - \mu_{gt}(t) - \mu_{gen}(t). \end{aligned}$$

According to (10)–(14), the composite time-varying failure rate and composite failure rate for the CCHP system can be obtained by using the following equations:

$$\lambda_4(t) = \lambda_{gt}(t) + \lambda_{gen}(t), \tag{21}$$

$$\mu_4 = \frac{\lambda_4(t)}{\left[\left(1 + \dfrac{\lambda_{gt}(t)}{\mu_{gt}}\right)\left(1 + \dfrac{\lambda_{gen}(t)}{\mu_{gen}}\right) - 1\right]}, \tag{22}$$

where $\lambda_4(t)$ is the composite time-varying failure rate for the CCHP system, μ_4 is the composite repair rate for the CCHP system. $\lambda_{gt}(t)$, μ_{gt}, $\lambda_{gen}(t)$ and μ_{gen} are the gas turbine and generator's time-varying failure and repair rates.

3.2.5. Markov model for the commercial power system

The Markov model for the commercial power system is presented in Fig. 6, where the failure and repair rates are denoted by λ_{cp} and μ_{cp}. The failure rate of the commercial power system is constant due to the guarantee of a steady electricity supply.

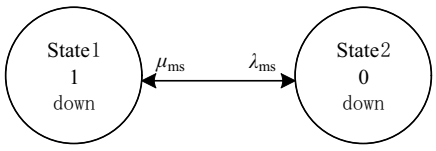

Fig. 6. Stochastic model for the commercial power system

3.3. Reliability indices of a port power system

Reliability is the probability that a power system will meet the load requirements by shifting the distribution power system from a single power source to a multiple power source. The reinforcement of the port distribution power system by integrating DG should be based on technical considerations. This will enhance the reliability of the power system and reduce the cost of energy. The performance metrics used for assessing the port power system include *FOR*, *LOLP* and *EENS*.

FOR is to assess the reliability of the generator set. *LOLP* is the expected time when the power is insufficient. It can judge that the installed capacity of the power system does not meet the required requirements. *EENS* is the common independent indicator in assessing the adequacy of large power grids. *EENS* integrates the frequency, duration of outages and the scale of outage events into an independent physical indicator. *EENS* can be combined with an appropriate power outage loss evaluation rate to estimate the user's power outage cost at the load point and the entire system. The reliability indices are briefly explained below. Their choice reflects the topology and operation states of the considered port power system and can verify the validity of the proposed model.

3.3.1. Force outage rate

The force outage rate (*FOR*) is the probability of forced outage with the power generation equipment, reflecting the generator set's reliability. The *FOR* can be expressed as:

$$r = \frac{\lambda(t)}{\lambda(t) + \mu}, \tag{23}$$

where $\lambda(t)$ and μ are the power generation's time-varying failure and repair rates.

3.3.2. Loss of load probability

The loss of load probability *(LOLP)* is the probability that the available capacity of power generation is less than or equal to constant load demand. The *LOLP* is a measure of the time when the power system's installed capacity cannot meet the demand. The *LOLP* of a power system can be estimated by (24).

$$LOLP = \sum_k p_k t_k, \tag{24}$$

where t_k is the time and p_k is the accumulated state probability.

3.3.3. Expectation energy not supplied

The expected energy not supplied (*EENS*) is the expected value of power shortage due to the forced outage of generating units in a power system. The utilities use this index for the reliability assessment of a power system. The *EENS* can be calculated by using the following mathematical expressions:

$$EENS = \sum_L \sum_R^C (X - R) p(X), \tag{25}$$

where L is the hourly load during the period, X is the outage capacity of the power system, R is the reserve capacity of the

power system, and $p(X)$ is the exact probability of the outage capacity.

4. RESULTS AND ANALYSIS

The reliability assessment technique applied in this part is to assess the impact of using the solar, wind, ESS and CCHP in the conventional port distribution system. The model developed as a part of the study was implemented for the IEEE 34 Node Test Feeder system, as shown in Fig. 7. The system consists of 15 loads 34 feeders. The voltage of this distribution system is 1 kV. The detailed information about the specifications of the components, the reliability data and load for the IEEE 34 Node Test Feeder are presented in Tables 1, 2 and 3. Nine combinations are presented in Table 4 to study their effects on the reliability of the port distribution system. The specifications of these case studies are given below:

- Reliability indices calculation for different combinations of the port distribution system.
- DG system with different capacities is installed at bus 28.
- Combination 6 is installed at bus 3, bus 8, bus 28 and bus 31, respectively.

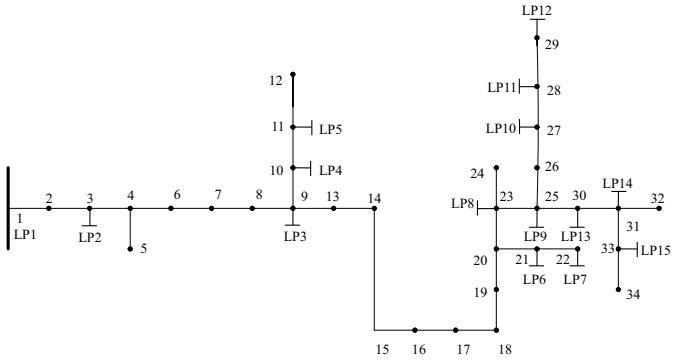

Fig. 7. Single line diagram of IEEE Test Feeder

Table 1
Specifications of the components of DG system [29]

Description	Solar	Wind	ESS	CCHP
Installed capacity	0.1 MW	0.2 MW	0.05 MW	0.1 MW
Efficiency	18.70%	45%	80–95%	80%
Other technical parameters	$V_{oc} = 22.30$ V, $I_{sc} = 11.89$ A, $V_{mp} = 18.0$ V, $I_{mp} = 11.2$ A, $K_i = 0.1\%/°C$, $K_v = 0.38/°C$, $T_a = 30°C$, $N_{ot} = 43°C$	$v_{ci} = 3$ m/s, $v_r = 10$ m/s, $v_{co} = 25$ m/s		

Case study 1: The reliability assessment is carried out on the modified IEEE Test Feeder with the application of nine combinations presented in Table 4. Figure 8 shows different configurations of the DG system using Markov models to analyze the force outage rate of the new energy units. The *FOR* of CCHP is the lowest, while the force outage rate of wind is the highest among these new energy units. Therefore, CCHP is better for reliability than the wind unit.

The solar system, wind system and CCHP system with different capacities are respectively installed on the IEEE 34 Node Test Feeder system, where the installed capacities of solar, wind and CCHP system are 0.1–0.6 MW. The value of *EENS* for the different capacities are obtained as shown in Fig. 9.

Table 2
Reliability data of different components of DG system [30]

Description	Average failure rate (failure/year)	Repair rate (repair/year)
PV	0.04	18.25
Wind turbine generator	0.05	20
Battery	0.0312	51.9671
Gas turbine	0.016	21.9
Generator	0.016	21.9
DC/DC boost converter	0.0657	62.5
DC/AC inverter	0.143	52.143
AC/DC rectifier	0.152	55.253
Charger controller	0.125	45.213

Table 3
Load data for the IEEE 34 Node Test Feeder

Description	Symbol	Power rating (MW)
Load points	LP1 and LP15	0.02
	LP2-LP6, LP10 and LP12-LP14	0.01
	LP11	0.15
	LP7	0.03
	LP8-LP9	0.05

Table 4
Different combinations for the port DG system

Combinations	Commercial power	Solar	Wind	ESS	CCHP
1	√				
2	√	√			
3	√		√		
4	√	√		√	
5	√		√	√	
6	√	√	√	√	
7	√	√		√	√
8	√		√	√	√
9	√	√	√	√	√

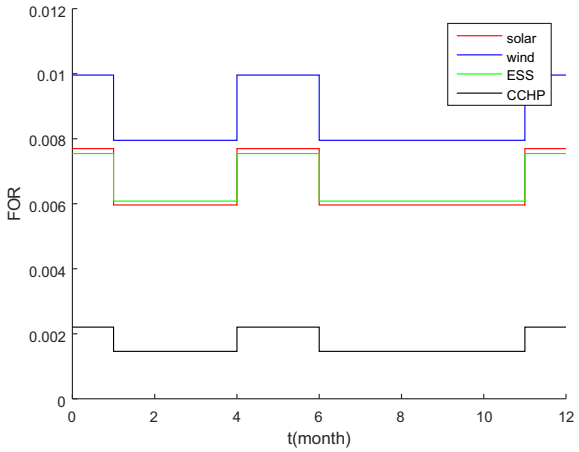

Fig. 8. Force outage rate of the DG system

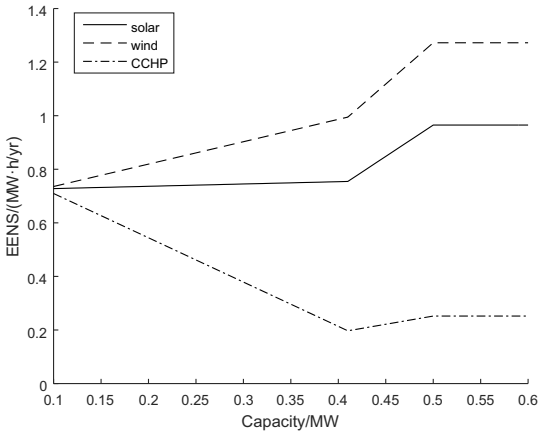

Fig. 9. The *EENS* values of solar, wind and CCHP system

When the IEEE 34 Node Test Feeder system is installed only with the solar system, the value of *EENS* increases slowly with an increase in the solar system capacity. When the solar system capacity increases to a certain extent, the value of *EENS* increases rapidly until it stabilizes. This phenomenon is because the solar system supplies the most power supply of the IEEE 34 Node Test Feeder system.

Conversely, when the IEEE 34 Node Test Feeder system is installed only with the wind system, the value of *EENS* increases gradually with the increase of the solar system capacity greater than the value of *EENS* of the wind system. When the wind system capacity increases to a certain extent, the value of *EENS* also increases rapidly until it stabilizes.

Compared with the solar and wind system, the *EENS* value of CCHP system decreases quickly with increasing CCHP system capacity. When the CCHP system capacity increases to a certain amount, the value of *EENS* increases slowly until it stabilizes.

The reliability of the CCHP system is better than that of solar and wind systems. The impact of the solar system on the reliability of the IEEE 34 Node Test Feeder system is relatively stable. Moreover, the installed capacity affects the reliability of the entire system. Appropriate installation capacity is conducive to improving the reliability of the entire system. Also, installing a single energy system to an integrated energy system will seriously affect its reliability.

The solar, wind and CCHP system combined with different ESS system capacities are respectively installed on the IEEE 34 Node Test Feeder system, where the installed capacities of ESS system are 0.05–0.15 MW. The value of *EENS* for the different capacities are obtained as shown in Fig. 10.

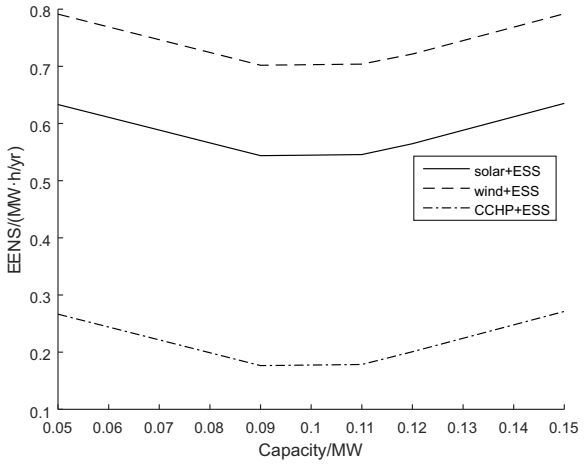

Fig. 10. The *EENS* values of solar, wind and CCHP system combined with different capacities of ESS system

As seen from Fig. 10, when the installed capacity of the ESS system reaches about 20% of the entire system, the *EENS* value of the solar, wind and CCHP system combined with ESS system capacities all reach the minimum value. This shows that installing an ESS system with a suitable capacity can greatly improve the reliability of the entire system.

The value of *EENS* of the CCHP system combined with the ESS system decreased significantly by about 30%, achieving optimal reliability. The *EENS* value of the wind system combined with ESS system decreased by only about 10%. It has the least improvement on the entire system reliability.

The integration of the nine combinations into the conventional port distribution system has changed the values of the reliability indices, as shown in Table 5. The values of *LOLP*

Table 5
Results for the port distributions

Combination	*LOLP* (d/yr)	*EENS* (MW·h/yr)
1	2.2680	0.9299
2	4.6071	0.7280
3	5.3518	0.8194
4	4.6071	0.6161
5	5.3518	0.7078
6	7.6705	0.5085
7	5.2142	0.3963
8	5.9575	0.4882
9	6.6506	0.4135

for the distribution system reliability indices with combination 2–9 are increased by 2.3391, 3.0838, 2.3391, 3.0838, 5.4025, 2.9462, 3.6895 and 4.3826, respectively and are more than that of the conventional power system. This increases the probability that power generation's available capacity is less than or equal to constant demand. The results in Table 5 show that the system's reliability has improved. The value of *EENS* for the distribution system with combination 2–9 is improved by 20.19%, 11.88%, 33.75%, 23.88%, 45.32%, 57.38%, 47.50% and 55.53%. The reliability of this new distributed power system has been greatly improved compared to the conventional power system.

To study the influence of different locations of DG on the entire system reliability, the DG system is connected to nodes 3, 8, 28 and 31 of the IEEE 34 Node Test Feeder system, respectively. The system indices, i.e. *SAIFI*, *SAIDI*, *ASAI*, are shown in Table 6.

As can be seen from the data, the values of *SAIFI* and *SAIDI* decrease as the access location of DG system is closer to the end of IEEE 34 Node Test Feeder system. The best values of *SAIFI* and *SAIDI* are obtained for the DG system connecting to node 31, as shown in Table. 6. The values of *SAIFI* and *SAIDI* are very close when the DG system is connected to nodes 28 and 31, respectively. The reliability of the entire system has improved when the DG system is connected to node 28 or 31 of IEEE 34 Node Test Feeder system, where the closest load point is large.

Table 6
System indices for a different location

Location	*SAIFI* (f/c·yr)	*SAIDI* (h/c·yr)	ASAI
No DG	0.704	3.52	0.999598
Node 3 + DG	0.665	3.325	0.99962
Node 8 + DG	0.593	2.965	0.999662
Node 28 + DG	0.5567	2.78	0.999683
Node 31 + DG	0.5435	2.72	0.999689

Case study 2: The voltage profile of the IEEE Test Feeder at bus 28 for all combinations is shown in Fig. 11. The voltage is 5.34% lower in the conventional port distribution power system without new energy units. The voltage is improved due to the contribution of the DG system, but it varies for different combinations. Combinations 6 and 9 seem to be the best solutions compared with other combinations.

The IEEE 34 Node Test Feeder losses are presented in Fig. 12. The losses of the conventional port distribution system are the highest and reach 0.02164 MW. The losses of the DG system reach their minimum value of 0.00042 MW for Combination 8, while the loss of the distribution power system increases to 0.0012 MW for Combination 9 because of increasing capacity. This shows that increasing the capacity of the DG system does not always reduce losses. The above analysis shows that integrating the new energy DG units in the port distribution power system can increase the reliability and efficiency of the system.

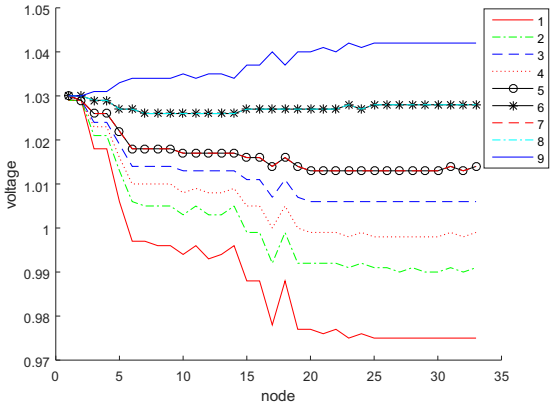

Fig. 11. Voltage profiles for all combinations

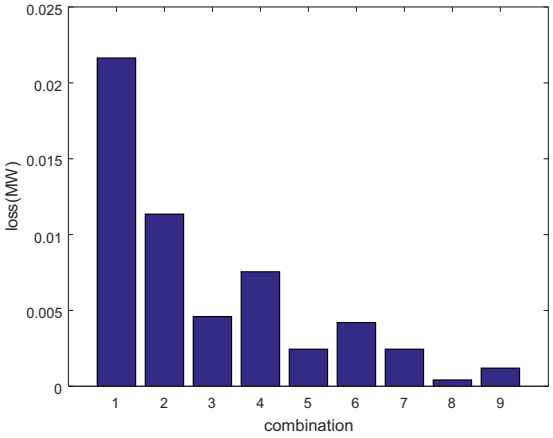

Fig. 12. Loss for all combinations

Case study 3: The port power system integrating the combination 6 unit in the port distribution power system at nodes 3, 8, 28 and 31 is considered. The voltage varies significantly at different nodes, as shown in Fig. 13. The voltage drops by 4.37% at node 3 when the DG system is installed at the first end of the lines. Installing the DG system at node 8 improves the voltage slightly. The voltage enhancement at nodes 28 and 31 is better than that obtained at other nodes due to heavy load.

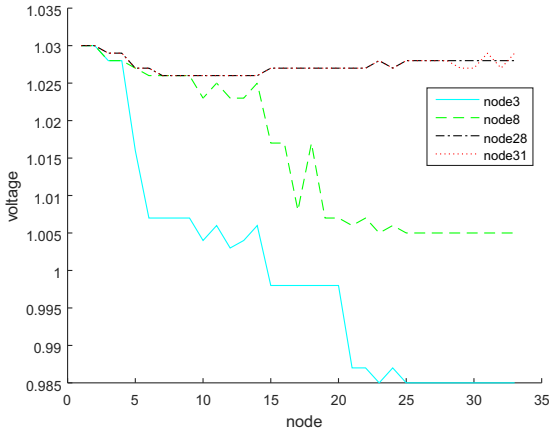

Fig. 13. Voltage profiles for node 3, 8, 28 and 31

The losses of the IEEE 34 Node Test Feeder at all nodes are shown in Fig. 14. The losses of the lines are the lowest when the DG system is installed near node 28, representing areas with many electrical devices. This illustrates that appropriate location of the new energy units can reduce the losses.

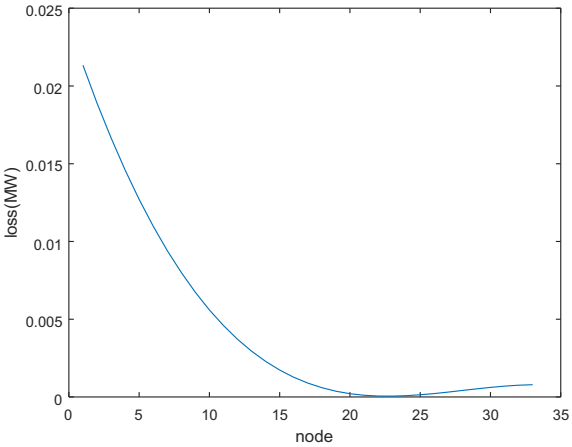

Fig. 14. Loss for all node of IEEE Test Feeder

5. CONCLUSIONS

The introduction of solar, wind, ESS and CCHP systems into the port distribution power system is key for improving its reliability. The reliability assessment based on Markov chains applied to the IEEE 34 Node Test Feeder proved that the integration of DG significantly increases reliability indices, reduces undervoltage and minimizes losses when applied at proper locations and with proper capacities. The proposed approach overcomes the limitations and difficulties associated with evaluating the reliability of complex power systems, which can be used to optimally locate and size DG into the port power system to enhance its reliability and performance.

Future work will be extended to consider various cold ironing schemes. Future ships can also be considered a hybrid system with DGs and energy storage facilities. Therefore, future ports can be treated as a cluster of microgrids. This opens up new opportunities for energy management in the systems. Ships berthing in the port could simply provide emergency energy for the port system or additional energy storage capabilities.

ACKNOWLEDGEMENTS

Shanghai S&T Commission partially supported this work under Grant 19040501700, the Sino-Polish S&T Cooperation Project 37-11, Shanghai Belt and Road Joint Laboratory in SMU.

REFERENCES

[1] T. Song, Y. Li, X. Zhang, C. Wu, J. Li, Y. Guo, and H. Gu, "Integrated port energy system considering integrated demand response and energy interconnection," *Int. J. Electr. Power Energy Syst.*, vol. 117, no. 1, p. 1055654, 2020, doi: 10.1016/j.ijepes.2019.105654.

[2] G. Parise, L. Parise, L. Martirano, P. Chavdarian, C-L. Su, and A. Ferrante, "Wise Port and Business Energy Management: Port Facilities, Electrical Power Distribution," *IEEE Trans. Ind. Appl.*, vol. 52, no. 1, pp. 18–24, 2016, doi: 10.1109/TIA.2015.2461176.

[3] L. Alhmoud and B. Wang, "A review of the state-of-the-art in wind-energy reliability analysis," *Renew. Sustain. Energy Rev.*, vol. 81, no.2, pp. 1643–1651, 2018, doi: 10.1016/j.rser.2017.05.252.

[4] J. Chen, T. Yu, Y. Xu, X. Cheng, B. Yang, and B. Zhen, "Fast analytical method for reliability evaluation of electricity-gas integrated energy system considering dispatch strategies," *Appl. Energy*, vol. 242, no. 2, pp. 260–272, 2019, doi: 10.1016/j.apenergy.2019.03.106.

[5] T. Adefarati, and R. Bansal, "The impacts of PV-wind-diesel-electric storage hybrid system on the reliability of a power system," *Energy Procedia*, vol. 105, pp. 616–621, 2017, doi: 10.1016/j.egypro.2017.03.364.

[6] M. Ahmadi, O. Adewuyi, M. Danish, P. Mandal, A. Yona, and T. Senjyu, "Optimum coordination of centralized and distributed renewable power generation incorporating battery storage system into the electric distribution network," *Int. J. Electr. Power Energy Syst.*, vol. 125, p. 106458, 2021, doi: 10.1016/j.ijepes.2020.106458.

[7] G. Li, R. Zhang, T. Jiang, H. Chen, L. Bai, and X. Li, "Security-constrained bi-level economic dispatch model for integrated natural gas and electricity systems considering wind power and power-to-gas process," *Appl. Energy*, vol. 194, pp. 696–704, 2017, doi: 10.1016/j.apenergy.2016.07.077.

[8] C. Wang, S. Liu, Z. Bie, and J. Wang, "Renewable Energy Accommodation Capability Evaluation of Power System with Wind Power and Photovoltaic Integration," *IFAC-PapersOnLine*, vol. 51, no. 28, pp. 55–60, 2018, doi: 10.1016/j.ifacol.2018.11.677.

[9] B. Das, M. Alotaibi, P. Das, M. Islam, S. Das, M Hossain, "Feasibility and techno-economic analysis of stand-alone and grid-connected PV/Wind/Diesel/Batt hybrid energy system: A case study," *Energy Strategy Rev.*, vol. 37, p. 100673, 2021, doi: 10.1016/j.esr.2021.100673.

[10] T. Agajie, B. Khan, J. Guerrero, and O. Mahela, "Reliability enhancement and voltage profile improvement of distribution network using optimal capacity allocation and placement of distributed energy resources," *Comput. Electr. Eng.*, vol. 93, pp. 1–22, 2021, doi: 10.1016/j.compeleceng.2021.107295.

[11] H. Nejad, S. Tavakoli, N. Ghadimi, S. Korjani, S. Nojavan, and H. Didani, "Reliability based optimal allocation of distributed generations in transmission systems under demand response program," *Electr. Power Syst. Res.*, vol. 176, pp. 1–10, 2019, doi: 10.1016/j.epsr.2019.105952.

[12] D. Almeida, C. Borges, G. Oliveira, and M. Pereira, "Multi-area reliability assessment based on importance sampling, MCMC and stratification to incorporate variable renewable sources," *Electr. Power Syst. Res.*, vol. 193, no. 4, pp. 1–12, 2021, doi: 10.1016/j.epsr.2020.107001.

[13] Y. Wang, X. Han, and Y. Ding, "Power system operational reliability equivalent modeling and analysis based on the Markov chain," in Proc. of 2012 *IEEE Int. Conf. Power System Techn. (POWERCON)*, 2012, pp. 1–5, doi: 10.1109/PowerCon.2012.6401316.

[14] M. Al-Muhaini and G. Heydt, "A novel method for evaluating future power distribution system reliability," *IEEE Trans. Power Syst.*, vol. 28, no. 3, pp. 3018–3027, 2013, doi: 10.1109/TPWRS.2012.2230195.

[15] Z. Abdmouleh, A. Gastli, L. Ben-Brahim, M. Haouari, and N. Al-Emadi, "Review of optimization techniques applied for the integration of distributed generation from renewable energy sources," *Renew. Energy*, vol. 113, pp. 266–280, 2017, doi: 10.1016/j.renene.2017.05.087.

[16] F. Lamzouri, E. Boufounas, and A. Ei Amrani, "Efficient energy management and robust power control of a stand-alone wind-photovoltaic hybrid system with battery storage," *J. Energy Storage*, vol. 42, pp. 1–18, 2021, doi: 10.1016/j.est.2021.103044.

[17] M. Qaisrani, J. Wei, L. Ali-Khan, "Potential and transition of concentrated solar power: A case study of China," *Sustain. Energy Technol. Assess.*, vol. 44, no. 205, 2021, doi: 10.1016/j.seta.2021.101052.

[18] A. Allouhi, "A novel grid-connected solar PV-thermal/ wind integrated system for simultaneous electricity and heat generation in single family buildings," *J. Clean. Prod.*, vol. 6, 2021, doi: 10.1016/j.jclepro.2021.128518.

[19] R. Zhang, and H. Zhang, "Research on the application of solar photovoltaic power generation in port," *Pearl River Water Transport*, vol. 11, pp. 23–25, 2015.

[20] E. Saretta, P. Caputo, and F. Frontini, "A review study about energy renovation of building facades with BIPV in urban environment," *Sustain. Cities Soc.*, vol. 44, pp. 343–355, 2019, doi: 10.1016/j.scs.2018.10.002.

[21] H. Lan, S. Wen, Y. Hong, D. Yu, and L. Zhang, "Optimal sizing of hybrid PV/diesel/battery in ship power system," *Appl. Energy*, vol. 158, pp. 26–34, 2015, doi: 10.1016/j.apenergy.2015.08.031.

[22] D. Lamsal, V. Sreeram, Y. Mishra, and D. Kumar, "Output power smoothing control approaches for wind and photovoltaic generation systems: A review," *Renew. Sust. Energ. Rev.*, vol. 113, no. 12, pp. 1–22, 2019, doi: 10.1016/ j.rser.2019.109245.

[23] Y-L. Wang *et al.*, "Research on capacity planning and optimization of regional integrated energy system based on hybrid energy storage system," *Appl. Therm. Eng.*, vol. 180, no. 6390, p. 115834, 2020, doi: 10.1016/j.applthermaleng.2020.115834.

[24] A. Malheiro, P. Castro, R. Lima, A. Estanqueiro, "Integrated sizing and scheduling of wind/PV/diesel/battery isolated systems," *Renew. Energy*, vol. 83, pp. 646–657, 2015, doi: 10.1016/j.renene.2015.04.066.

[25] S. Afzali, and V. Mahalec, "Novel performance curves to determine optimal operation of CCHP systems," *Appl. Energy*, vol. 226, pp. 1009–1036, 2018, doi: 10.1016/j.apenergy.2018.06.024.

[26] C-Y. Zheng, J-Y. Wu, X-Q. Zhai, and R-Z. Wang, "A novel thermal storage strategy for CCHP system based on energy demands and state of storage tank," *Int. J. Electr. Power Energy Syst.*, vol. 85, no. 4, pp. 117–129, 2017, doi: 10.1016/j.ijepes.2016.08.008.

[27] Z. Han, L-T. Tian, and L. Cheng, "A deducing-based reliability optimization for electrical equipment with constant failure rate components duration their mission profile," *Reliab. Eng. Syst. Safety*, vol. 212, no. 2, pp. 1–10, 2021, doi: 10.1016/j.ress.2021.107575.

[28] M. Almuhaini and A. Al-Sakkaf, "Markovian model for reliability assessment of microgrids considering load transfer restriction," *Turk. J. Elec. Eng. & Comp. Sci.*, vol. 25, no. 6, pp. 4657–4672, 2017, doi: 10.3906/elk-1609-137.

[29] A. Kaabeche and R. Ibtiouen, "Techno-economic optimization of hybrid photovoltaic/wind/ diesel/battery generation in a stand-alone power system," *Solar Energy*, vol. 103, pp. 71–82, 2014, doi: 10.1016/j.solener.2014.02.017.

[30] T. Adefarati and R. Bansal, "Reliability and economic assessment of a microgrid power system with the integration of renewable energy resources," *Appl. Energy*, vol. 206, pp. 911–933, 2017, doi: 10.1016/j.apenergy.2017.08.228.